Zero-field NMR and NQR measurements of the antiferromagnet $URhIn_5$

H. Sakai,[1,*] S. Kambe,[1] Y. Tokunaga,[1] Y. Matsumoto,[1] N. Tateiwa,[1] Y. Haga,[1] and Z. Fisk[1,2]
[1]*Advanced Science Research Center, Japan Atomic Energy Agency, Tokai, Ibaraki 319-1195, Japan*
[2]*Department of Physics and Astronomy, University of California, Irvine, California 92697, USA*
(Received 8 May 2013; published 19 July 2013)

The antiferromagnet $URhIn_5$ with the Néel temperature $T_N = 98$ K has been investigated by nuclear magnetic/quadrupole resonance (NMR/NQR). ^{115}In-NQR spectra in the paramagnetic state give the respective electrical field gradient parameters for the locally tetragonal and orthorhombic In(1) and In(2) sites. In the antiferromagnetic state at 4.5 K, ^{115}In-NMR spectra in the zero external field indicate a commensurate antiferromagnetic structure. The internal field at In(1) sites is found to be zero and that at In(2) sites is 21.1 kOe at 4.5 K. The temperature (T) dependence of the nuclear relaxation rates $1/T_1$ in the paramagnetic state shows a distinct site dependence: Korringa-type constant $(T_1T)^{-1}$ behavior below ~150 K for In(1) sites and a divergent behavior of $1/T_1$ toward T_N for In(2). The plausible antiferromagnetic structure is discussed based on these observations.

DOI: 10.1103/PhysRevB.88.045123 PACS number(s): 75.25.−j, 76.60.Gv

I. INTRODUCTION

The large family of "115" intermetallic compounds with tetragonal $HoCoGa_5$ type has opened an interesting avenue in the field of strongly correlated f electron systems.[1] The successive discovery of the plutonium superconductors $PuCoGa_5$ (Ref. 2) and $PuRhGa_5$ (Ref. 3) with transition temperatures $T_c = 18$ and 9 K, respectively, sparked interest in the actinide-based ($An115$) compounds $AnTGa_5$ (An = U, Np, Pu; T = transition-metal elements). The isomorphic indium compound $PuCoIn_5$ has been recently reported to be a new superconductor with $T_c = 2.5$ K.[4] In the closely related isostructural heavy-fermion Ce115 series $CeTIn_5$ (T = Co, Rh, Ir), $CeCoIn_5$ and $CeIrIn_5$ become superconducting below 2.3 and 0.4 K, respectively.[5–7] $CeRhIn_5$, an antiferromagnet with Néel temperature $T_N = 3.8$ K at ambient pressure, becomes superconducting near 2 K, with suppression of the antiferromagnetism, at applied pressure of $P^* \sim 2$ GPa.[8] Systematic nuclear magnetic resonance (NMR) investigations of the Ce115 systems have established that these superconductors have d-wave superconducting gaps,[9–12] and that antiferromagnetic (AFM) spin interactions play an active role in the superconducting pairing.[13–16] In the Pu115 systems, NMR measurements show d-wave-like superconducting gap behavior,[17,18] with T_c's an order of magnitude higher than those for the Ce115. In heavy-fermion 115 systems, recent systematic NMR experiments have suggested that AFM XY-type anisotropy is more favorable for d-wave superconductivity than Ising-type or isotropic fluctuations.[19–21] On the other hand, in the U115 and Np115 series, which are Pauli paramagnets or antiferromagnets, no superconductivity has been found.[22–34]

In U115 systems, only gallium compounds have been reported. A search for isomorphic U115 indium compounds succeeded in the discovery and growth of single crystals of $URhIn_5$.[35] $URhIn_5$ is found from measurement of resistivity, magnetic susceptibility, and specific heat to be an antiferromagnet with $T_N \sim 98$ K. In order to microscopically characterize the $5f$ electronic state in this new antiferromagnet $URhIn_5$, ^{115}In-NMR and nuclear quadruple resonance (NQR) measurements in zero field have been performed using approximately one dozen small single crystals. In Sec. II, the experimental details are given and the hyperfine parameters are defined. In Sec. III, we report the NQR spectra in the paramagnetic (PM) state, and the NMR spectra in zero field in the Néel state of $URhIn_5$. Nuclear relaxation rates $1/T_1$ in $URhIn_5$ are presented. Here, the apparent nature of $5f$ electrons in $URhIn_5$ is found to vary from rather localized for temperatures above ~150 K to itinerant for temperatures below ~150 K, i.e., the AFM state in $URhIn_5$ appears to be driven by itinerant $5f$ electrons. Finally, in Sec. IV, the possible AFM structure is discussed based on the NMR spectra for the respective In sites.

II. EXPERIMENTS

Single-crystal samples of $URhIn_5$ were prepared by the In-flux method.[35] For the NMR/NQR measurements, a dozen single crystals were used without grinding in order to avoid spectral broadening due to lattice distortions. NMR measurements were carried out in the temperature range 4–300 K using a phase-coherent, pulsed spectrometer installed in a special area for handling radioisotopes. Frequency-swept NMR/NQR spectra were measured in the zero field by stepwise summing of the spin-echo signal intensity with an autotuning NMR probe.

Both ^{113,115}In nuclei have nuclear spin $I = \frac{9}{2}$, so there are nuclear quadrupolar interactions. Using conventional notation, the quadrupole frequency parameter is defined as $\nu_Q \equiv \frac{3e^2qQ}{2I(2I-1)h}$, where eQ is the nuclear quadrupolar moment ($^{113,115}Q$ are given as 1.14 and 1.16, respectively), and $eq \equiv V_{ZZ}$ is the principal component of the electric field gradient (EFG) tensor. Here, V_{ii} denotes EFG tensor components in the principal coordinate system, such that $|V_{XX}| \leqslant |V_{YY}| \leqslant |V_{ZZ}|$ for each ionic site. The EFG components satisfy LaPlace's equation, i.e., $V_{XX} + V_{YY} + V_{ZZ} = 0$. The EFG asymmetry parameter is defined as $\eta \equiv \frac{|V_{YY}|-|V_{XX}|}{|V_{ZZ}|}$. The nuclear gyromagnetic ratio values used here are $^{115}\gamma_N/2\pi = 0.93301$ MHz/kOe for the major ^{115}In isotope with the natural abundance of 95.72%, while $^{113}\gamma_N/2\pi = 0.93099$ MHz/kOe for the minor isotope ^{113}In with a small abundance of 4.28%. Due to the small

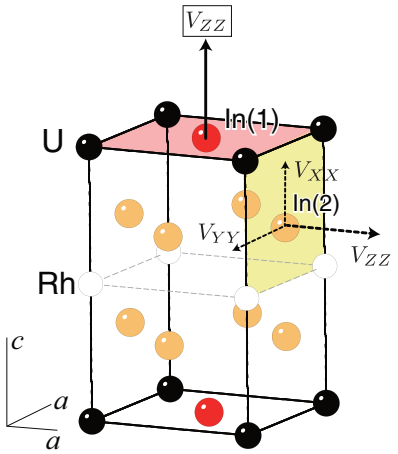

FIG. 1. (Color online) Crystal structure of $URhIn_5$. The local coordinates of the EFG on each In site are indicated.

abundance and closeness of γ_N and Q, the ^{113}In signal of ^{113}In is usually buried by the adjoining signal of the ^{115}In signal.

$URhIn_5$ crystallizes in the tetragonal $HoCoGa_5$-type structure (space group, $P4/mmm$), illustrated in Fig. 1. This crystal structure is quasi-two-dimensional in character, i.e., it can be regarded as a sequential stacking of UIn_3 and $RhIn_2$ layers along the c axis. There are two inequivalent crystallographic In sites: the locally tetragonal In(1) ($1c$ site) and the orthorhombic In(2) ($4i$ site), as shown in Fig. 1. Due to the local symmetry, the EFG asymmetry parameter η must be zero for In(1) and nonzero for In(2) sites. The local coordinates based on the principal axes of EFG can be determined, as denoted in Fig. 1: V_{ZZ} for In(1) is parallel to the c axis, and V_{ZZ} for In(2) is perpendicular to the ac plane and V_{XX} is parallel to the c axis. These local coordinates for each site in the 115 compounds are well established by symmetry and experimentally.[36]

The nuclear spin-lattice relaxation time T_1 was measured using the inversion-recovery method with a π pulse. Values of T_1 were obtained from fits to an appropriate relaxation function[37] for the In(1) and In(2) sites, respectively.

III. RESULTS

A. NQR spectra

Figure 2 displays all ^{115}In-NQR spectra for In(1) and In(2) sites in the PM state at 115 K in $URhIn_5$. The signal intensities are corrected by the frequencies squared to deduce the transition probabilities. Correction by nuclear spin-spin relaxation times T_2 is unnecessary since the data were taken with a very short separation τ of 12 μs between the first and second rf pulses. As shown in Figs. 2(b)–2(d), each line is quite sharp with linewidth of ~60 kHz. These sharp NQR lines indicate the high quality and homogeneity of the crystals. A weak resonance was also observed as denoted by the asterisk in Fig. 2(a), with two orders of magnitude longer nuclear relaxation time than the main signals. This is probably a small contribution from a nonmagnetic binary compound, e.g., Rh-In, although it could not be identified.

From crystallographic considerations, the assignments for In(1) and In(2) have been determined. The local tetragonal symmetry of In(1), i.e., $\eta = 0$, requires the NQR lines equally

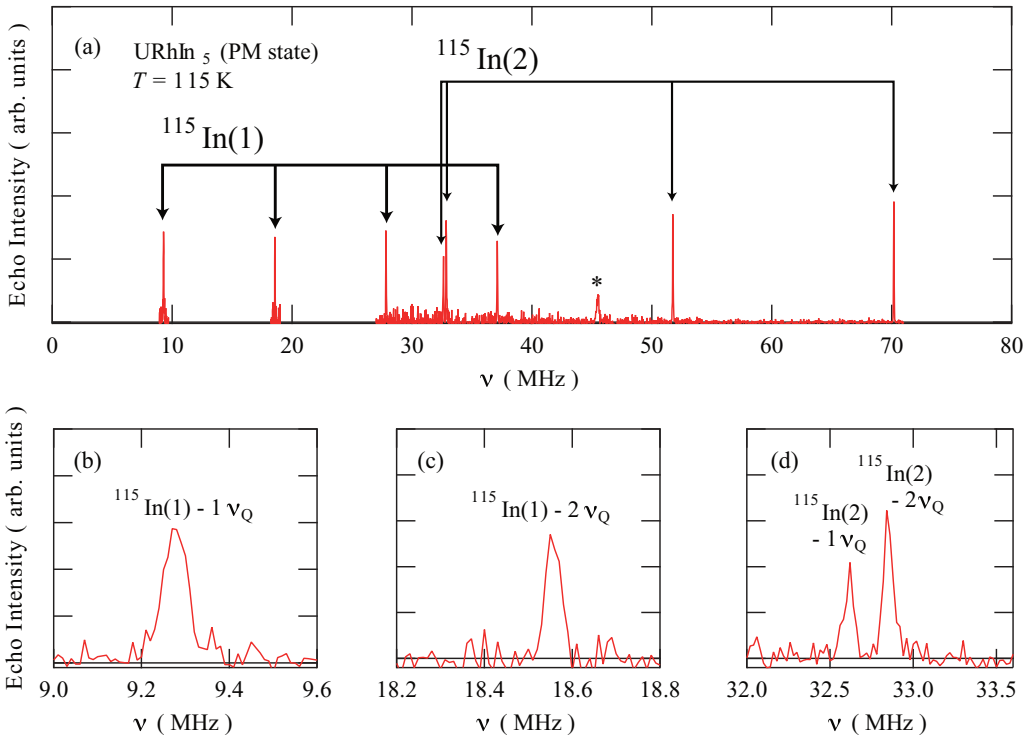

FIG. 2. (Color online) (a) ^{115}In-NQR spectra in zero external field for In(1) and In(2) sites in the PM state of $URhIn_5$ taken at 115 K. The assignments are also denoted by arrow sets. (b) and (c) are the expansions for each line for $1\nu_Q$ and $2\nu_Q$ of In(1) sites, and (d) for $1\nu_Q$ and $2\nu_Q$ of In(2) sites. The line marked by an asterisk could not be assigned.

separated in ν_Q, and the remaining four lines with high intensities then arise from In(2), as denoted in Fig. 2(a). Thus, the ν_Q for ^{115}In(1) is easily determined to be 9.276 MHz at 115 K. In the case of finite η, the following electric quadrupole Hamiltonian matrix

$$\mathcal{H}_Q = \frac{h\nu_Q}{6}\left\{3I_z^2 - I(I+1) + \frac{\eta}{2}(I_+^2 + I_-^2)\right\} \qquad (1)$$

can be diagonalized to obtain the EFG parameters. As usual, the four allowed ($\Delta m = \pm 1$) and the associated forbidden ($|\Delta m| > 1$) transitions would be observed if η is finite. In $URhIn_5$, however, only the four allowed transitions are observed, as seen similarly for the In(2) sites in Ce115 compounds. The numerical diagonalization has been done to fit the frequencies for these transitions. As a result, the ν_Q and η for ^{115}In(2) at 115 K are determined to be 17.74 MHz and 0.376, respectively. This ν_Q value is close to that of $CeIrIn_5$ [$\nu_Q = 18.1$ MHz (Ref. 9)] and somewhat larger than that of $CeCoIn_5$ [15.5 MHz (Ref. 9)] or $CeRhIn_5$ [16.665 MHz (Ref. 38)], while the η is close to that of $CeCoIn_5$ [$\eta = 0.39$ (Ref. 9)] and smaller than that of $CeIrIn_5$ [0.46 (Ref. 9)] and $CeRhIn_5$ [0.445 (Ref. 38)].

B. NMR spectra in zero field below T_N

Figure 3 shows the ^{115}In-NQR/NMR spectra in the AFM state of $URhIn_5$ at 4.5 K well below T_N, which is obtained by frequency sweep in the zero external field. It is noted that the fast repetition of pulses (~200 ms) weakened the signals coming from the nonmagnetic impurity (marked by the asterisk in Fig. 2). Therefore, all the visible resonance lines in Fig. 3 originate from ^{115}In in $URhIn_5$. Here, in order to compare with the simulated transition probabilities, the signal intensities were again divided by the carrier frequencies squared, but no T_2 correction was made since the τ was very short. The noisy background below ~30 MHz in Fig. 3 is due to this correction.

From Fig. 3, the AFM order is concluded to be commensurate since the spectral lines remain very sharp as seen in the PM state, i.e., no characteristic line broadening due to the distribution of internal fields by incommensurate AFM ordering, such as seen in the related materials $CeRhIn_5$ (Ref. 38) or $CePt_2In_7$ (Ref. 39).

The In(1) lines remain in the nearly same position as in the PM state relative to the simulated lines plotted together in Fig. 3, so these lines are NQR lines with no internal field on the In(1) sites. On the other hand, the NMR spectra for In(2) show a characteristic line splitting from NQR lines in the PM state. In the AFM state in zero external field, the NMR occurs by the internal (hyperfine) field H_{int} on the ligand In sites transferred from the magnetic uranium ions. In such a case, one needs to diagonalize the effective Hamiltonian matrix $\mathcal{H}_Z + \mathcal{H}_Q$ where $\mathcal{H}_Z = \gamma_N \hbar \boldsymbol{I} \cdot \boldsymbol{H}_{int}$ is the Zeeman term. As shown in Fig. 3, by fitting to the diagonalized resonances, the remaining spectra can be explained simply by taking $H_{int} = 21.1$ kOe, which is parallel to the V_{YY} on each In(2) site. We also note that any differing field orientation can not explain the experimental resonances. In this fitting procedure, ν_Q and η for In(2) are also obtained as shown in the following. The result is schematically illustrated in Fig. 4. The magnetic structure is discussed later in Sec. IV based on these experimental facts: (i) no internal field on the In(1) sites, and (ii) finite internal field with unique magnitude parallel to V_{YY} on the In(2) sites transferred from the uranium sites.

C. Temperature dependence of the internal field and EFG parameters

Figure 5 shows the temperature dependence of H_{int} on the In(2) sites. The dotted curve is a result fitted with $H_{int} \propto \{1 - (T/T_N)^\alpha\}^\beta$. The best fit gives $T_N = 98.2$ K, $\alpha = 3.9$, and

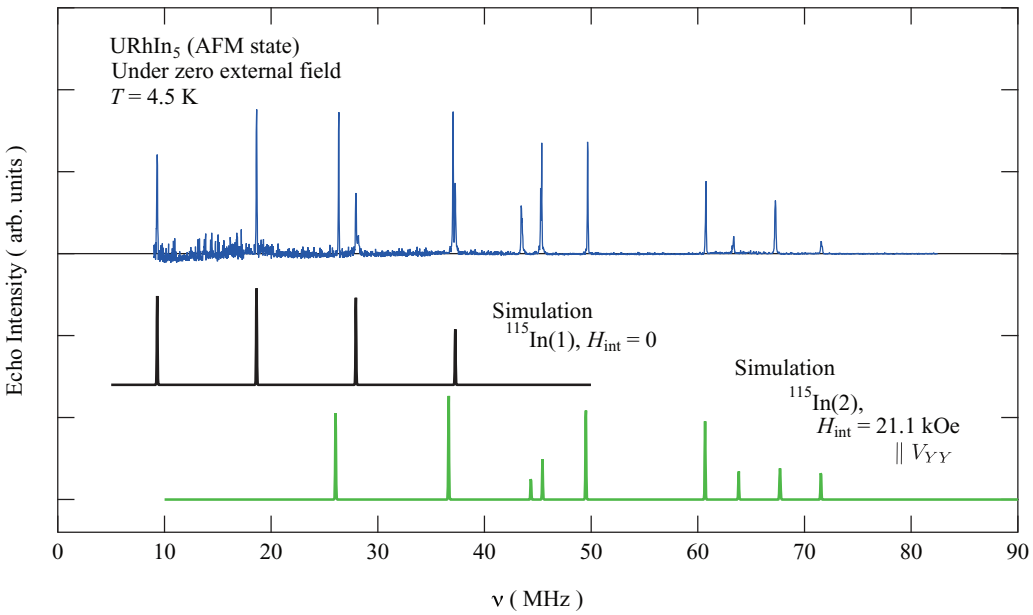

FIG. 3. (Color online) ^{115}In-NMR spectra in zero external field for the In(1) and In(2) sites in the AFM state of $URhIn_5$ taken at 4.5 K. The simulated resonance lines given by diagonalization of the effective Hamiltonian are also plotted for the In(1) and In(2) sites, respectively.

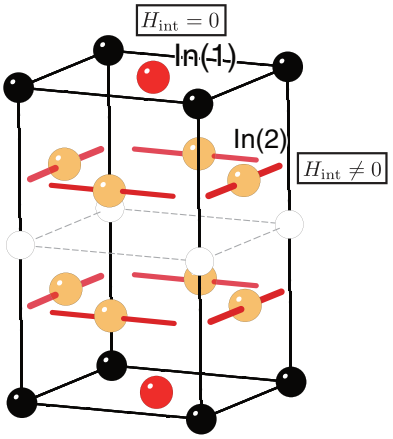

FIG. 4. (Color online) Schematic illustration to indicate by bold lines the directional axes of the (transferred) internal fields ($H_{\rm int}$) to the In(2) sites. The amplitude of $H_{\rm int}$ is unique on the In(2) sites. No internal field is transferred to the In(1) sites.

$\beta = 0.27$, respectively. The development of $H_{\rm int}$ just below $T_{\rm N}$ is found to vary more rapidly than the conventional mean field result. The saturated value of $H_{\rm int}$ can be estimated to be 21.1 kOe at $T \to 0$.

Figure 6 is the temperature dependence of $\nu_{\rm Q}$ for ^{115}In(1) and ^{115}In(2), and the EFG asymmetry parameter η for In(2) is inserted into the inset of Fig. 6(b). η is nearly T independent. In most PM solids, the temperature dependence arises from lattice vibrations (phonons) in which the phenomenological relation $\nu_{\rm Q}(T) \propto T^{3/2}$ generally holds.[40] In $URhIn_5$, however, this $T^{3/2}$ term is found to be very small. In particular, $\nu_{\rm Q}(T)$ for ^{115}In(1) appears to be nearly T linear as seen in Fig. 6(a). In order to fit the data in the PM region, the empirical formula $\nu_{\rm Q}(T) = \nu_{\rm Q0} + kT + lT^{3/2}$ is used. The obtained parameters for ^{115}In(1) and ^{115}In(2) are $\nu_{\rm Q0} = 9.39$ MHz, $k = -0.0014$ MHz/K, $l = 1 \times 10^{-5}$ MHz/K$^{3/2}$ and $\nu_{\rm Q0} = 17.89$ MHz, $k = -0.00075$ MHz/K, $l = -4 \times 10^{-5}$ MHz/K$^{3/2}$, respectively. The fits well reproduce the data in the PM region, as shown in Fig. 6. Interestingly, the $\nu_{\rm Q}(T)$ for In(1) below $T_{\rm N}$ shows an opposite tendency to that for In(2), i.e., a decrease of $\nu_{\rm Q}(T)$ for In(1) and an increase for In(2) from the extrapolated values. Because of the local symmetry, the $\nu_{\rm Q}$ for In(1) would vary as the linear thermal expansion along the

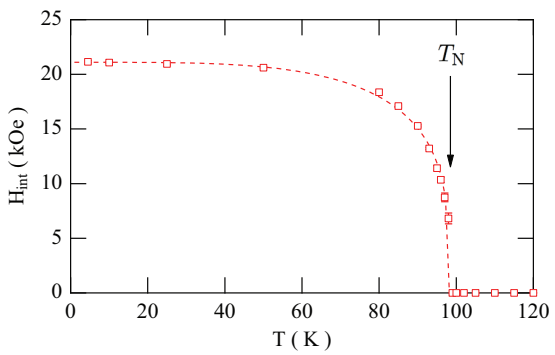

FIG. 5. (Color online) Temperature dependence of the internal field $H_{\rm int}$ on the In(2) sites. The dotted curve represents the fit with $H_{\rm int} \propto \{1 - (T/T_{\rm N})^{\alpha}\}^{\beta}$.

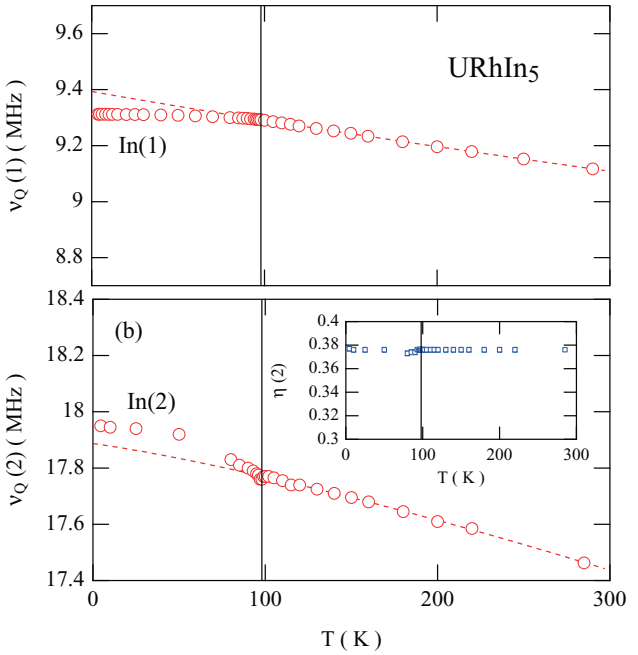

FIG. 6. (Color online) Temperature dependence of nuclear quadrupolar frequencies for (a) ^{115}In(1) and (b) ^{115}In(2) in $URhIn_5$. The inset in the bottom panel shows the temperature dependence of the EFG asymmetry parameter η on In(2) sites. The dotted curves represent the fit with $\nu_{\rm Q}(T) = \nu_{\rm Q0} + kT + lT^{3/2}$ in the PM region.

a axis and that for In(2) to those along both the a and c axes. Probably, the anisotropic $\Delta\nu_{\rm Q}(T)$ between In(1) and In(2) below $T_{\rm N}$ is associated with a characteristic magnetovolume effect in $URhIn_5$.

D. Nuclear relaxation rates

Figure 7 shows the temperature dependence of the nuclear spin-lattice relaxation rate $1/T_1$ measured at the NQR lines for In(1) in $URhIn_5$. Since the internal field is found to be canceled at the In(1) sites, the NQR lines remain even below $T_{\rm N}$. Therefore, $1/T_1$ below $T_{\rm N}$ can be determined using the identical nuclear magnetization recovery functions in the PM state. We also note that the values of $1/T_1$ for the $1\nu_{\rm Q}$, $2\nu_{\rm Q}$, $3\nu_{\rm Q}$, and $4\nu_{\rm Q}$ lines are equal at each temperature. In the PM region, the $1/T_1$ just above $T_{\rm N}$ is proportional to temperature, i.e., $(T_1T)^{-1}$ is constant in the temperature range from $T_{\rm N}$ to $T^* \sim 150$ K, as clearly seen in the inset of Fig. 7.

In general, $1/T_1$ on the ligand sites can be written as[41,42]

$$\frac{1}{T_1} = \frac{k_{\rm B}T}{(\gamma_{\rm e}\hbar)^2} \cdot 2(\gamma_{\rm n}A_{\perp})^2 \sum_{\boldsymbol{q}} f^2(\boldsymbol{q}) \frac{{\rm Im}\chi_{\perp}(\boldsymbol{q},\omega_0)}{\omega_0}, \qquad (2)$$

where $\gamma_{\rm n}$ and $\gamma_{\rm e}$ are the nuclear and electronic gyromagnetic ratios, A is the transferred hyperfine coupling constant, $f_{\alpha}(\boldsymbol{q})$ is the hyperfine form factor, ${\rm Im}\chi(\boldsymbol{q},\omega_0)$ is the imaginary part of dynamical susceptibility generated by magnetic atoms, ω_0 is the NQR frequency, and the suffix $\perp$ refers to the component perpendicular to the quantization axis. The hyperfine coupling constants mainly originate from the hybridization between U $5f$ and the ligand $5s/5p$. Therefore, the $\boldsymbol{q}$ dependence of the transferred hyperfine coupling is imposed by $f(\boldsymbol{q})$ since the transferred hyperfine fields are locally produced by the nearest

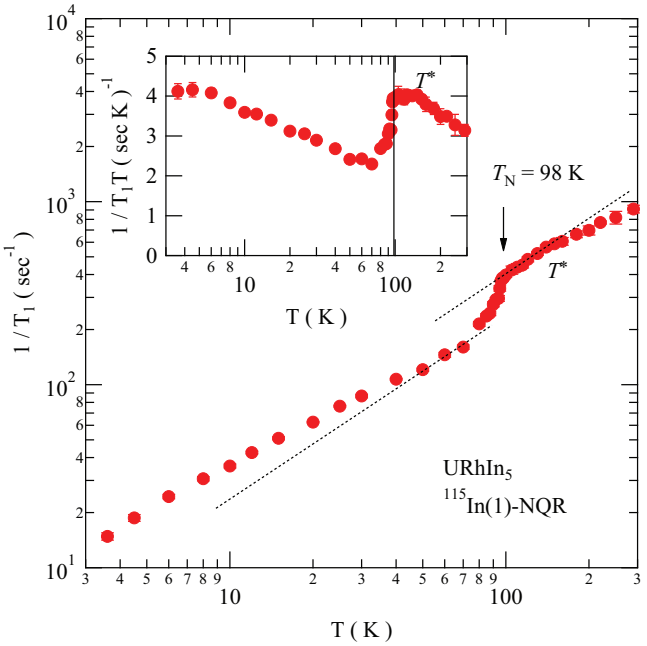

FIG. 7. (Color online) Temperature dependence of nuclear spin-lattice relaxation rate $1/T_1$ for In(1) in URhIn$_5$. Both axes are plotted on a logarithmic scale. The dotted lines are guides to the eye. The inset shows $1/T_1$ divided by temperature as a function of temperature for In(1) in URhIn$_5$. The semilogarithmic plot is displayed in the inset.

U ions. For example, $f^2(\boldsymbol{q}) = 16\cos^2(q_x a/2)\cos^2(q_y a/2)$ for the tetragonal In(1) sites. Indeed, $f^2(\boldsymbol{q}) = 0$ at the specific AFM propagation vector of $q_x = \pi/a$ or $q_y = \pi/a$, although the q dependence of $f^2(\boldsymbol{q})$ is weak trigonometrically. However, since spin fluctuations in the PM state usually have broad widths in $\boldsymbol{q}$ space, $(T_1T)^{-1}$ can sense AFM fluctuations beyond the moderate filtering by the trigonometrical $f^2(\boldsymbol{q})$ term. In the case of cubic UIn$_3$ with AFM propagation vector of $2\pi\,\boldsymbol{Q}/a \equiv (\pi/a,\pi/a,\pi/a)$, $1/T_1$ just above T_N can sense a critical increase of AFM fluctuations beyond such a $f^2(\boldsymbol{q})$ filtering.[43] Hereafter, since $f^2(\boldsymbol{q})$ is not important for the following discussions, $f^2(\boldsymbol{q})$ is assumed to be unity for simplicity. It is noted here that the simple approximation of neglecting the $\boldsymbol{q}$ dependence of $f^2(\boldsymbol{q})$ is more relevant to the In(2) sites since the site symmetry is lower and hyperfine fluctuations do not vanish at any particular field orientation. In this case, $f^2(\boldsymbol{q})$ becomes a more complicated trigonometrical function.[44]

An additional consequence from Eq. (2) is that $1/T_1$ is only sensitive to the perpendicular spin with respect to the quantization axis. Namely, $1/T_1$ for In(1)-NQR can detect the in-plane fluctuations only of $5f$ electrons since the quantization axis is the c axis parallel to the principal axis V_{ZZ} of the EFG. On the other hand, that for In(2)-NQR can sense the fluctuations both along the a and c axes because $V_{ZZ} \parallel a$. As shown in Fig. 8, $(T_1T)^{-1}$ measured for the In(2)-NQR line in URhIn$_5$ shows a critical increase just above T_N, while $(T_1T)^{-1}$ for In(1)-NQR does not exhibit such an enhancement. Therefore, the anisotropic AFM enhancement of $(T_1T)^{-1}$ between the ligand sites of In(1) and In(2) originates from the strong $5f$ fluctuations along the c axis, i.e., the ordered moment in the AFM state tends to be orientated along the c axis. Such an anisotropic AFM enhancement due to a tendency for c-oriented moments is also detected by NMR $1/T_1$ measurements in NpCoGa$_5$.[36]

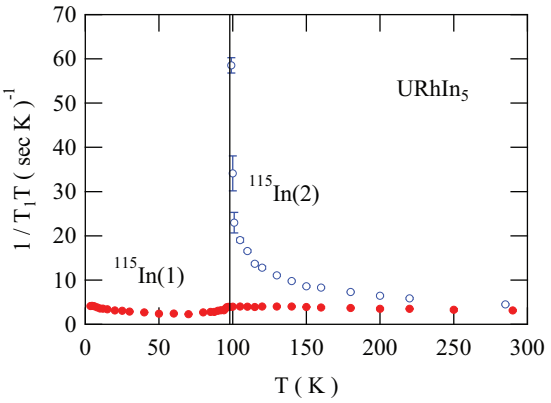

FIG. 8. (Color online) Temperature dependence of nuclear spin-lattice relaxation rate divided by temperature $(T_1T)^{-1}$ for In(1) and In(2) in URhIn$_5$.

If itinerant electrons dominate the magnetic relaxation, in an electron gas model, the q summation of the imaginary part of dynamical susceptibility becomes $\sum_q \mathrm{Im}\chi(q,\omega) = \pi\gamma_e^2 \iint d\varepsilon\, d\varepsilon' \delta(\varepsilon - \varepsilon' - \omega) N(\varepsilon) N(\varepsilon')[f(\varepsilon) - f(\varepsilon')]$, with $\hbar$ and k_B as unity, where $f(x)$ and $N(x)$ are the Fermi distribution function and density of states. Then, from Eq. (2), $(T_1T)^{-1}$ becomes T independent (the so-called Korringa behavior) and the value of $(T_1T)^{-1}$ is proportional to the square of $N(E_F)$. Even if electronic correlations exist, $(T_1T)^{-1}$ is proportional to $N^2(E_F)$ and the magnetic correlation factor $\mathcal{K}(\alpha)$ as long as the random-phase approximation (RPA) is applicable.[42] In the case with localized character, $1/T_1$ is known to reach a constant value.[41] Such a constant behavior of $1/T_1$ in the localized regime has been observed in the paramagnetic state of UIn$_3$.[43]

Since a constant behavior of $(T_1T)^{-1}$ is clearly observed below $T^* \sim 150$ K, $5f$ electrons acquire itinerant character by hybridization with conduction electrons below T^*, although the AFM enhancement factor $\mathcal{K}(\alpha)$ is uncertain. Above T^*, $1/T_1$ for In(1) deviates downward and that for In(2) reaches a constant behavior, indicating a loss of $5f$ electrons' itinerancy. As evidence that $1/T_1$ for In(1) reacts to the $5f$ magnetism, a drop of $1/T_1$ just below T_N is observed, corresponding to a decrease of the density of states (DOS) at the Fermi surface after the AFM ordering opens an energy gap. Since there is no reason for the correlation factor $\mathcal{K}(\alpha)$ to increase below T_N after AFM ordering, the unusual increase of $(T_1T)^{-1}$ below $\sim$50 K (see the inset of Fig. 7) should be attributed to a recovery of the DOS at the Fermi surface at temperatures well below T_N. We note that $(T_1T)^{-1}$ seems to saturate at the lowest temperature near 4 K, as seen in the inset of Fig. 7. Such a recovery feature of DOS below T_N may be connected with AFM nesting effects on the Fermi surface, which would cause an increase of the residual DOS by self-polarization of up- and down-spin bands.

IV. DISCUSSION

The experimental results are briefly enumerated.

(1) The AFM propagation vector is commensurate.

(2) No internal field is transferred to the In(1) sites.

(3) Finite internal fields with unique magnitude parallel to V_{YY} are transferred to the In(2) sites from the uranium sites as illustrated in Fig. 4.

(4) PM moments on the U sites tend to orient parallel to the c axis.

(5) AFM ordering is driven by itinerant $5f$ electrons hybridized with conduction electrons below $T^* \sim 150$ K.

A plausible AFM structure in $URhIn_5$ can be proposed based on the results 1–3 of the static spectral information. First, item 1 makes the puzzle simple: we can conclude that neither spin density wave nor incommensurate spiral AFM as observed in $CeRhIn_5$ (Ref. 45) occurs in $URhIn_5$, i.e., all the U atoms carry the same moment μ_{ord} with a simple AFM arrangement. Therefore, we need only determine the simple AFM propagation vectors which reproduce the observed internal fields on the ligand sites. From item 2, we can conclude that the AFM propagation vector should have an in-plane component at least, i.e., $q_x = \pi/a$ and/or $q_y = \pi/a$, because an in-plane ferromagnetic arrangement of $q_x = q_y = 0$ should give a finite internal field at the In(1) sites. Thus, the possible AFM propagation vectors are narrowed to $\boldsymbol{Q}_0 = (\frac{1}{2},0,0)$, $\boldsymbol{Q}_1 = (\frac{1}{2},0,\frac{1}{2})$, $\boldsymbol{Q}_2 = (\frac{1}{2},\frac{1}{2},0)$, or $\boldsymbol{Q}_3 = (\frac{1}{2},\frac{1}{2},\frac{1}{2})$.

The internal fields at nonmagnetic ligand sites originate from the spin-density distribution of magnetic ions through the dipolar and transferred hyperfine interactions. In principle, if the complete hyperfine tensor was determined in the ordered state through quantification of the c-f mixing effect, the internal fields could be calculated assuming possible magnetic structures. In many cases, however, the hyperfine coupling tensor in the ordered state can not be resolved experimentally. Instead, even without such a complete solution, we can deduce possible directions for the internal field at a nonmagnetic ligand site on the basis of symmetry:[46–49] *the induced magnetic field at a ligand site never breaks the symmetry of the magnetic sublattice*.

Let us consider the in-plane μ_{ord} cases to begin with. If μ_{ord} were parallel to the a axis, any simple AFM propagation vector can not give a unique magnitude of the internal field parallel to the V_{YY} axis at the In(2) site by this symmetry principle because such an AFM structure breaks the fourfold-rotational symmetry leading to at least two kinds of hyperfine fields at the In(2) sites in magnitude or in direction. This situation is the same even if the μ_{ord} is parallel to $\langle 110\rangle$ with in-plane stripe type $\boldsymbol{Q}_0$ or $\boldsymbol{Q}_1$. Only in the case of μ_{ord} parallel to $\langle 110\rangle$ with $\boldsymbol{Q}_2$ or $\boldsymbol{Q}_3$ do the two kinds of hyperfine fields on the In(2) sites accord in magnitude and direction. But, it is parallel to the c axis, i.e., V_{XX}. These are inconsistent with item 3. Based on the foregoing considerations, even more general cases of $\mu_{ord} \parallel \langle uv0\rangle$ ($u,v \neq 0,1$ and $u \neq v$) with AFM arrangement even including multi-k cases (noncollinear AFM structure) can not give a solution with a unique $|H_{int}| \parallel V_{YY}$ on the In(2) sites. Similarly, the case of $\mu_{ord} \parallel \langle uvw\rangle$ ($u,v,w \neq 0$) is also impossible for explaining the observed internal fields at the In(2) sites.

As a consequence, symmetry considerations preclude the possibility of in-plane μ_{ord}, i.e., the ordered moments μ_{ord} on U sites must be parallel to the c axis. This is also consistent with item 4 from $1/T_1$ as well. In the AFM structure of $\boldsymbol{Q}_0$, $\boldsymbol{Q}_1$, $\boldsymbol{Q}_2$, or $\boldsymbol{Q}_3$ with $\mu_{ord} \parallel c$, as shown in Figs. 9(a) –9(d),

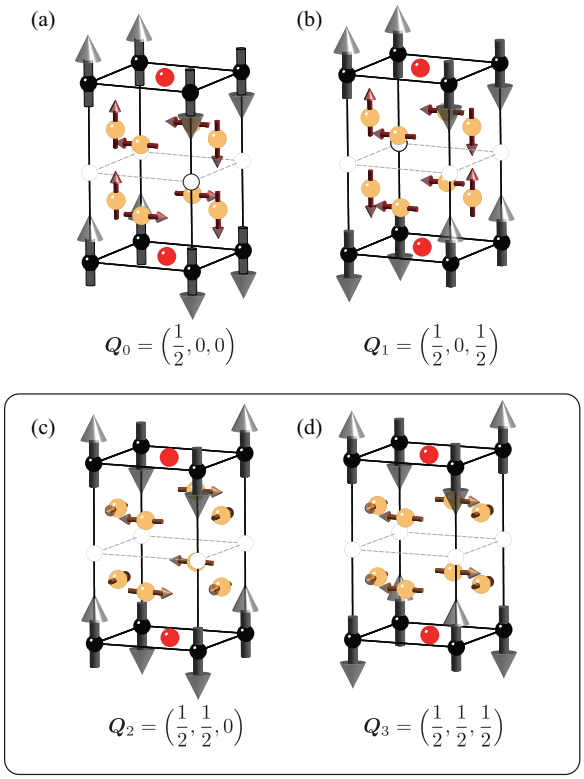

FIG. 9. (Color online) Possible AFM structures for $URhIn_5$ assuming an ordered moment parallel to the c axis. The bold arrows represent the ordered moments on U sites. The directions of hyperfine fields on the In(2) sites are also illustrated by thin arrows. In these structures, no internal field is transferred onto the In(1) sites.

the possible directions of hyperfine fields on the In(2) sites are already discussed in our previous works for $NpFeGa_5$ (Ref. 48) and $TbCoGa_5$ (Ref. 49). For example, in the case of $\boldsymbol{Q}_0$ or $\boldsymbol{Q}_1$ as shown in Figs. 9(a) and 9(b), the In(2) sites magnetically split into two sites again from the differing local directions of H_{int}, i.e., one is parallel to V_{XX} and another is parallel to V_{YY}. Of course, this is also inconsistent with the experimental observation. Therefore, a possible AFM structure for $URhIn_5$ consistent with items 1–3 requires either $\boldsymbol{Q}_2$ or $\boldsymbol{Q}_3$ with Ising-type moments along the c axis in view of the symmetry requirement, as shown in Figs. 9(c) and 9(d). For further identification via NMR, however, ^{103}Rh-NMR ($I = \frac{1}{2}$) experiments will be necessary with external fields. If the local field on the Rh sites is transferred (or canceled), the AFM structure can be determined by which of the two possibilities is realized.

Next, we roughly estimate the size of ordered moments assuming a similar hyperfine coupling constant to that in related UIn_3. In UIn_3, the hyperfine coupling $A_\perp$ is experimentally obtained as 54 kOe/μ_B in the PM state.[43] In this case, $A_\perp$ is produced mainly by four nearest-neighbor U atoms, while the $A_\perp$ on the In(2) sites in $URhIn_5$ comes from two nearest neighbors. So, assuming half of $A_\perp$, the size of the ordered moment in $URhIn_5$ can be roughly estimated to be $\sim 1\ \mu_B$/U from $H_{int} = 21.1$ kOe on the In(2) sites. This value is quite reduced from the $\sim 3.6\ \mu_B$ of the U^{3+} or U^{4+} free ion. This reduction of the ordered moment is consistent with item 5 in the experimental results. Regarding item 5, we also note that the resistivity as well as the susceptibility show a broad hump

around T^* with increasing temperature above T_N, indicating development of c-f hybridization around T^*.[35]

Finally, the lattice properties of $URhIn_5$ can be examined to check consistency with the possible AFM structures. Above all, it should be noted that there is no compound having the same AFM structure of $\boldsymbol{Q}_2 = (\frac{1}{2},\frac{1}{2},0)$ with $\mu_{ord} \parallel c$ among the antiferromagnets of the $Ln115$ (Ln = Ce, Nd, Tb, Dy, Ho) and $An115$ (An = U, Np) family, so far as we know. On the other hand, the same AFM structure of $\boldsymbol{Q}_3 = (\frac{1}{2},\frac{1}{2},\frac{1}{2})$ with c-oriented moments has been found in the related compound $UNiGa_5$.[23] Systematic neutron diffraction studies of the antiferromagnets $UTGa_5$ (T = Ni, Pd, Pt) with c-directed ordered moments[50] reveal that a local tetragonal factor defined by $t \equiv 1-(2cz/a)$ can predict the stable AFM structure, where z is the positional parameter of the crystallographic In(2) sites $(0,\frac{1}{2},z)$. The local tetragonal factor t represents the local compression of U-In cages along the c axis. The t for $URhIn_5$ determined by x-ray diffraction is $\sim$3.1% near T_N, which is closer to the 1.7% seen in $UNiGa_5$ with $\boldsymbol{Q}_3$ than the 5.4% seen in $UPdGa_5$ with a different $\boldsymbol{Q}_4 = (0,0,\frac{1}{2})$, and much smaller than the 7% seen in $UPtGa_5$ with $\boldsymbol{Q}_4$. Characteristically, the basal plane lattice constant a for $URhIn_5$ contracts below T_N (Ref. 35) as seen in $UNiGa_5$, while it is known to expand in $UPtGa_5$.[50] Thus, the magnetic response of lattice in $URhIn_5$ may suggest a similar AFM structure to $UNiGa_5$.

V. SUMMARY

We have performed NQR/NMR measurement in the zero external field for single crystals of the antiferromagnet $URhIn_5$ with $T_N = 98$ K. The complete In-NQR spectra have been obtained. The NMR spectra below T_N can be interpreted with no internal field on the In(1) sites and a finite internal field on the In(2) sites parallel to the local V_{YY} axis of the EFG. The nuclear spin-lattice relaxation rates $1/T_1$ indicate that the AFM state is driven by itinerant $5f$ electrons, which are hybridized with conduction electrons below $T^* \sim 150$ K. The difference in $1/T_1$ between In(1) and In(2) sites indicates that the ordered moments have an Ising character along the c axis. A recovery of DOS well below T_N is indicated by a gradual increase of $(T_1T)^{-1}$, which may be connected with Fermi-surface properties of $URhIn_5$.

From our results and lattice properties, the AFM structure in $URhIn_5$ appears to be the same AFM structure found in $UNiGa_5$. The most plausible AFM structure in $URhIn_5$ is $\boldsymbol{Q}_3 = (\frac{1}{2},\frac{1}{2},\frac{1}{2})$ in Fig. 9(d). In order to completely identify this structure, the further ^{103}Rh-NMR experiment will be performed with external fields in the near future. A complementary neutron diffraction study will be necessary as well.

ACKNOWLEDGMENTS

We would like to thank K. Kaneko, N. Metoki, T. D. Matsuda, D. Aoki, Y. Ōnuki, and H. Yasuoka for stimulating discussions and suggestions. Part of this work was supported by a Grant-in-Aid for Scientific Research on Innovative Areas Heavy Electrons (Grants No. 20102006 and No. 20102007) by the MEXT of Japan. This research was also partially supported by the REIMEI Research Program of JAEA.

*sakai.hironori@jaea.go.jp

[1] J. D. Thompson and Z. Fisk, J. Phys. Soc. Jpn. **81**, 011002 (2012).
[2] J. L. Sarrao, L. A. Morales, J. D. Thompson, B. L. Scott, G. R. Stewart, F. Wastin, J. Rebizant, P. Boulet, E. Colineau, and G. H. Lander, Nature (London) **420**, 297 (2002).
[3] F. Wastin, P. Boulet, J. Rebizant, E. Colineau, and G. H. Lander, J. Phys.: Condens. Matter **15**, S2279 (2003).
[4] E. D. Bauer, M. M. Altarawneh, P. H. Tobash, K. Gofryk, O. E. Ayala-Valenzuela, J. N. Mitchell, R. D. McDonald, C. H. Mielke, F. Ronning, J.-C. Griveau, E. Colineau, R. Eloirdi, R. Caciuffo, B. L. Scott, O. Janka, S. M. Kauzlarich, and J. D. Thompson, J. Phys.: Condens. Matter **24**, 052206 (2012).
[5] C. Petrovic, P. G. Pagliuso, M. F. Hundley, R. Movshovich, J. L. Sarrao, J. D. Thompson, Z. Fisk, and P. Monthoux, J. Phys.: Condens. Matter **13**, L337 (2001).
[6] C. Petrovic, R. Movshovich, M. Jaime, P. G. Pagliuso, M. F. Hundley, J. L. Sarrao, Z. Fisk, and J. D. Thompson, Europhys. Lett. **53**, 354 (2001).
[7] R. Movshovich, M. Jaime, J. D. Thompson, C. Petrovic, Z. Fisk, P. G. Pagliuso, and J. L. Sarrao, Phys. Rev. Lett. **86**, 5152 (2001).
[8] H. Hegger, C. Petrovic, E. G. Moshopoulou, M. F. Hundley, J. L. Sarrao, Z. Fisk, and J. D. Thompson, Phys. Rev. Lett. **84**, 4986 (2000).
[9] Y. Kohori, Y. Yamato, Y. Iwamoto, T. Kohara, E. D. Bauer, M. B. Maple, and J. L. Sarrao, Phys. Rev. B **64**, 134526 (2001).
[10] G.-q. Zheng, K. Tanabe, T. Mito, S. Kawasaki, Y. Kitaoka, D. Aoki, Y. Haga, and Y. Ōnuki, Phys. Rev. Lett. **86**, 4664 (2001).
[11] N. J. Curro, B. Simovic, P. C. Hammel, P. G. Pagliuso, J. L. Sarrao, J. D. Thompson, and G. B. Martins, Phys. Rev. B **64**, 180514 (2001).
[12] T. Mito, S. Kawasaki, G.-q. Zheng, Y. Kawasaki, K. Ishida, Y. Kitaoka, D. Aoki, Y. Haga, and Y. Ōnuki, Phys. Rev. B **63**, 220507 (2001).
[13] N. J. Curro, J. L. Sarrao, J. D. Thompson, P. G. Pagliuso, Š. Kos, A. Abanov, and D. Pines, Phys. Rev. Lett. **90**, 227202 (2003).
[14] S. Kawasaki, T. Mito, Y. Kawasaki, G.-q. Zheng, Y. Kitaoka, D. Aoki, Y. Haga, and Y. Ōnuki, Phys. Rev. Lett. **91**, 137001 (2003).
[15] S. Kawasaki, G.- q. Zheng, H. Kan, Y. Kitaoka, H. Shishido, and Y. Ōnuki, Phys. Rev. Lett. **94**, 037007 (2005).
[16] M. Yashima, S. Kawasaki, Y. Kawasaki, G. -q. Zheng, Y. Kitaoka, H. Shishido, R. Settai, Y. Haga, and Y. Ōnuki, J. Phys. Soc. Jpn. **73**, 2073 (2004).
[17] N. J. Curro, T. Caldwell, E. D. Bauer, L. A. Morales, M. J. Graf, Y. Bang, A. V. Balatsky, J. D. Thompson, and J. L. Sarrao, Nature (London) **434**, 622 (2005).
[18] H. Sakai, Y. Tokunaga, T. Fujimoto, S. Kambe, R. E. Walstedt, H. Yasuoka, D. Aoki, Y. Homma, E. Yamamoto, A. Nakamura, Y. Shiokawa, K. Nakajima, Y. Arai, T. D. Matsuda, Y. Haga, and Y. Ōnuki, J. Phys. Soc. Jpn. **74**, 1710 (2005).

[19]S. Kambe, H. Sakai, Y. Tokunaga, T. Fujimoto, R. E. Walstedt, S. Ikeda, D. Aoki, Y. Homma, Y. Haga, Y. Shiokawa, and Y. Ōnuki, Phys. Rev. B **75**, 140509(R) (2007).
[20]H. Sakai, S. Kambe, Y. Tokunaga, Y. Haga, S.-H. Baek, F. Ronning, E. D. Bauer, and J. D. Thompson, Mater. Res. Soc. Symp. Proc. **1264**, 69 (2010).
[21]S.-H. Baek, H. Sakai, E. D. Bauer, J. N. Mitchell, J. A. Kennison, F. Ronning, and J. D. Thompson, Phys. Rev. Lett. **105**, 217002 (2010).
[22]Y. Tokiwa, S. Ikeda, Y. Haga, T. Okubo, T. Iizuka, K. Sugiyama, A. Nakamura, and Y. Ōnuki, J. Phys. Soc. Jpn. **71**, 845 (2002).
[23]Y. Tokiwa, Y. Haga, N. Metoki, Y. Ishii, and Y. Ōnuki, J. Phys. Soc. Jpn. **71**, 725 (2002).
[24]Y. Tokiwa, T. Maehira, S. Ikeda, Y. Haga, E. Yamamoto, A. Nakamura, Y. Ōnuki, M. Higuchi, and A. Hasegawa, J. Phys. Soc. Jpn. **70**, 2982 (2001).
[25]S. Ikeda, Y. Tokiwa, T. Okubo, Y. Haga, E. Yamamoto, Y. Inada, R. Settai, and Y. Ōnuki, J. Nucl. Sci. Technol. (Suppl.) **3**, 206 (2002).
[26]S. Ikeda, T. D. Matsuda, Y. Haga, E. Yamamoto, M. Nakashima, S. Kirita, T. C. Kobayashi, M. Hedo, Y. Uwatoko, H. Yamagami, H. Shishido, T. Ueda, R. Settai, and Y. Ōnuki, J. Phys. Soc. Jpn. **74**, 2277 (2005).
[27]S. Ikeda, Y. Tokiwa, T. D. Matsuda, A. Galatanu, E. Yamamoto, A. Nakamura, Y. Haga, and Y. Ōnuki, Phys. B (Amsterdam) **359-361**, 1039 (2005).
[28]E. Colineau, P. Javorský, P. Boulet, F. Wastin, J. C. Griveau, J. Rebizant, J. P. Sanchez, and G. R. Stewart, Phys. Rev. B **69**, 184411 (2004).
[29]D. Aoki, Y. Homma, Y. Shiokawa, H. Sakai, E. Yamamoto, A. Nakamura, Y. Haga, R. Settai, and Y. Ōnuki, J. Phys. Soc. Jpn. **74**, 2323 (2005).
[30]F. Honda, N. Metoki, K. Kaneko, D. Aoki, Y. Homma, E. Yamamoto, Y. Shiokawa, Y. Ōnuki, E. Colineau, N. Bernhoeft, and G. H. Lander, Phys. B (Amsterdam) **359-361**, 1147 (2005).
[31]F. Honda, N. Metoki, K. Kaneko, S. Jonen, E. Yamamoto, D. Aoki, Y. Homma, Y. Shiokawa, and Y. Ōnuki, Phys. B (Amsterdam) **378-380**, 1009 (2006).
[32]S. Jonen, N. Metoki, F. Honda, K. Kaneko, D. Aoki, Y. Homma, E. Yamamoto, Y. Haga, Y. Shiokawa, and Y. Ōnuki, Phys. B (Amsterdam) **378-380**, 1018 (2006).
[33]F. Honda, N. Metoki, K. Kaneko, S. Jonen, E. Yamamoto, D. Aoki, Y. Homma, Y. Haga, Y. Shiokawa, and Y. Ōnuki, Phys. Rev. B **74**, 144413 (2006).
[34]S. Jonen, N. Metoki, F. Honda, K. Kaneko, E. Yamamoto, Y. Haga, D. Aoki, Y. Homma, Y. Shiokawa, and Y. Ōnuki, Phys. Rev. B **74**, 144412 (2006).
[35]Y. Matsumoto, Y. Haga, N. Tateiwa, H. Sakai, T. D. Matsuda, E. Yamamoto, and Z. Fisk, Phys. Rev. B **88**, 045120 (2013).
[36]H. Sakai, S. Kambe, Y. Tokunaga, T. Fujimoto, R. E. Walstedt, H. Yasuoka, D. Aoki, Y. Homma, E. Yamamoto, A. Nakamura, Y. Shiokawa, and Y. Ōnuki, Phys. Rev. B **76**, 024410 (2007).
[37]J. Chepin and J. J. H. Ross, J. Phys.: Condens. Matter **3**, 8103 (1991).
[38]N. J. Curro, P. C. Hammel, P. G. Pagliuso, J. L. Sarrao, J. D. Thompson, and Z. Fisk, Phys. Rev. B **62**, R6100 (2000).
[39]H. Sakai, Y. Tokunaga, S. Kambe, H. O. Lee, V. A. Sidorov, P. H. Tobash, F. Ronning, E. D. Bauer, and J. D. Thompson, Phys. Rev. B **83**, 140408(R) (2011).
[40]E. N. Kaufmann and R. J. Vianden, Rev. Mod. Phys. **51**, 161 (1979).
[41]T. Moriya, Prog. Theor. Phys. **16**, 23 (1956); **16**, 641 (1956).
[42]T. Moriya, J. Phys. Soc. Jpn. **18**, 516 (1963).
[43]H. Sakai, S. Kambe, Y. Tokunaga, H. Chudo, Y. Tokiwa, D. Aoki, Y. Haga, Y. Ōnuki, and H. Yasuoka, Phys. Rev. B **79**, 104426 (2009).
[44]S. Kambe, H. Sakai, Y. Tokunaga, and R. E. Walstedt, Phys. Rev. B **82**, 144503 (2010).
[45]W. Bao, P. G. Pagliuso, J. L. Sarrao, J. D. Thompson, Z. Fisk, J. W. Lynn, and R. W. Erwin, Phys. Rev. B **62**, R14621 (2000).
[46]S. Demuynck, L. Sandratskii, S. Cottenier, J. Meersschaut, and M. Rots, J. Phys.: Condens. Matter **12**, 4629 (2000).
[47]T. Ohama, M. Hirano, and S. Noguchi, Phys. Rev. B **71**, 094408 (2005).
[48]S. Kambe, H. Sakai, Y. Tokunaga, R. E. Walstedt, D. Aoki, Y. Homma, and Y. Shiokawa, Phys. Rev. B **76**, 144433 (2007).
[49]Y. Tokunaga, Y. Saito, H. Sakai, S. Kambe, N. Sanada, R. Watanuki, K. Suzuki, Y. Kawasaki, and Y. Kishimoto, Phys. Rev. B **84**, 214403 (2011).
[50]K. Kaneko, N. Metoki, N. Bernhoeft, G. H. Lander, Y. Ishii, S. Ikeda, Y. Tokiwa, Y. Haga, and Y. Ōnuki, Phys. Rev. B **68**, 214419 (2003).